NASA/TM-20260000084

Thermoplastic Matrix Composite Design for Cryotanks Using Multiscale Modeling and Bayesian Optimization

Brandon L. Hearley, Brett A. Bednarcyk, Brooke R. Weborg,
Rula M. Coroneos, Evan J. Pineda, and Joshua Stuckner
Glenn Research Center, Cleveland, Ohio

August T. Noevere
Collier Aerospace Corp., Newport News, Virginia

January 2026

NASA STI Program Report Series

Since its founding, NASA has been dedicated to the advancement of aeronautics and space science. The NASA scientific and technical information (STI) program plays a key part in helping NASA maintain this important role.

The NASA STI program operates under the auspices of the Agency Chief Information Officer. It collects, organizes, provides for archiving, and disseminates NASA's STI. The NASA STI program provides access to the NTRS Registered and its public interface, the NASA Technical Reports Server, thus providing one of the largest collections of aeronautical and space science STI in the world. Results are published in both non-NASA channels and by NASA in the NASA STI Report Series, which includes the following report types:

- TECHNICAL PUBLICATION.
  Reports of completed research or a major significant phase of research that present the results of NASA programs and include extensive data or theoretical analysis. Includes compilations of significant scientific and technical data and information deemed to be of continuing reference value. NASA counterpart of peer-reviewed formal professional papers but has less stringent limitations on manuscript length and extent of graphic presentations.

- TECHNICAL MEMORANDUM.
  Scientific and technical findings that are preliminary or of specialized interest, e.g., quick release reports, working papers, and bibliographies that contain minimal annotation. Does not contain extensive analysis.

- CONTRACTOR REPORT.
  Scientific and technical findings by NASA-sponsored contractors and grantees.

- CONFERENCE PUBLICATION.
  Collected papers from scientific and technical conferences, symposia, seminars, or other meetings sponsored or cosponsored by NASA.

- SPECIAL PUBLICATION.
  Scientific, technical, or historical information from NASA programs, projects, and missions, often concerned with subjects having substantial public interest.

- TECHNICAL TRANSLATION.
  English-language translations of foreign scientific and technical material pertinent to NASA's mission.

Specialized services also include organizing and publishing research results, distributing specialized research announcements and feeds, providing information desk and personal search support, and enabling data exchange services.

For more information about the NASA STI program, see the following:

- Access the NASA STI program home page at http://www.sti.nasa.gov

NASA/TM-20260000084

Thermoplastic Matrix Composite Design for Cryotanks Using Multiscale Modeling and Bayesian Optimization

Brandon L. Hearley, Brett A. Bednarcyk, Brooke R. Weborg,
Rula M. Coroneos, Evan J. Pineda, and Joshua Stuckner
Glenn Research Center, Cleveland, Ohio

August T. Noevere
Collier Aerospace Corp., Newport News, Virginia

National Aeronautics and
Space Administration

Glenn Research Center
Cleveland, Ohio 44135

January 2026

Level of Review: This material has been technically reviewed by technical management.

This report is available in electronic form at https://www.sti.nasa.gov/ and https://ntrs.nasa.gov/

NASA STI Program/Mail Stop 050
NASA Langley Research Center
Hampton, VA 23681-2199

Thermoplastic Matrix Composite Design for Cryotanks Using Multiscale Modeling and Bayesian Optimization

Brandon L. Hearley, Brett A. Bednarcyk, Brooke R. Weborg,
Rula M. Coroneos, Evan J. Pineda, and Joshua Stuckner
National Aeronautics and Space Administration
Glenn Research Center
Cleveland, Ohio 44135

August T. Noevere
Collier Aerospace Corp.
Newport News, Virginia 23606

Abstract

Designing lightweight, robust cryogenic storage tanks is critical for future launch vehicles, in-space propellant storage, and hydrogen powered aircraft. This work presents a multiscale modeling and Bayesian optimization framework for the design of thermoplastic matrix composite cryotanks. Molecular dynamics simulations are first used to determine temperature-dependent constituent properties for candidate thermoplastic matrices, which are homogenized to the lamina scale using NASA's Multiscale Analysis Tool (NASMAT). These lamina properties, in combination with laminate family generation rules, are evaluated in HyperX structural optimization software to identify stacking sequences that meet all cryogenic load requirements. A Bayesian optimization framework is applied, with HyperX in the loop (via the HyperX API) to efficiently search across material and laminate design variables, yielding an optimized cryotank configuration with significant reductions in design cycle time compared to exhaustive search approaches.

Introduction

The development of advanced composite cryogenic tanks is a key enabler for next-generation launch vehicles and long-duration space missions. They are also candidates for hybrid electric aircraft vehicle fuel storage. Cryotanks must safely store propellants such as liquid hydrogen (LH_2) at temperatures approaching −253 °C while withstanding high internal pressures, repeated thermal cycles, and microcracking tendencies. Traditional metallic cryotanks are reliable but heavy, and cryogenic thermoset-based composites, while lighter, face challenges in matrix brittleness, permeability, and damage accumulation at extreme temperatures [1]. Thermoplastic matrix composites (TMCs) have emerged as a promising alternative due to their toughness, crack-arresting capability, and reparability, making them attractive candidates for cryogenic applications.

A central difficulty in designing composite cryotanks is the wide range of length scales and disciplines that must be integrated into the process. Material selection begins at the molecular level, where polymer chemistry determines stiffness, yield strength, and thermal expansion. These constituent properties propagate to the lamina level through fiber–matrix interactions and then to the laminate level, where ply stacking sequence governs the overall performance of the structure under realistic load cases. Microcracking and permeability further complicate laminate design, since ply-to-ply orientation changes that are tolerable at ambient conditions may be unacceptable under cryogenic thermal contraction. Advanced modeling approaches that couple atomistic simulations, micromechanics, finite element analysis, and structural optimization are therefore necessary to determine optimized cryotank configurations.

When designing a structural component for any aerospace application, minimizing weight while meeting all load requirements is paramount. When using composite laminates, weight savings can be achieved by dropping plies in regions where expected loading is not as critical as other regions of the structure. To ensure load transfer between ply-drop regions, at least one continuous ply must exist between the two laminate sections. Given a main stacking sequence (i.e., the stacking sequence of the region with the largest number of plies), candidate laminates for ply-drop regions can be determined by creating a laminate family, in which each subsequent laminate in the family is created by dropping plies from the previous laminate, ensuring compatibility and load transfer between regions.

Bayesian optimization (BO) provides an efficient method for exploring large design spaces where high-fidelity evaluations are expensive. Rather than exhaustively searching every possible combination of material, ply angle increment, and laminate configuration, BO leverages surrogate models and adaptive sampling to balance exploration of uncertain regions with exploitation of promising candidates [2]. Recent studies have demonstrated the effectiveness of BO for materials discovery and design automation, highlighting its potential for accelerating aerospace composite optimization [3, 4]. By coupling BO with existing structural sizing tools such as HyperX [5], it becomes possible to not only down-select layup configurations within a laminate family, but also optimize the laminate families themselves.

This work presents an integrated framework for polymer thermoplastic matrix composite cryotank design that combines multiscale modeling with Bayesian optimization. At the lowest length scale, properties of neat thermoplastics at room and cryogenic temperatures resulting from molecular dynamics simulations are employed. These constituent-level properties are homogenized to the ply level with NASA's Multiscale Analysis Tool (NASMAT) [6]. Laminate families are generated with custom stacking sequence rules designed to minimize ply-to-ply mismatch and permeability at cryogenic temperatures, and structural optimization is performed with HyperX. Finally, a global Bayesian optimization loop is employed to identify the optimal matrix material, laminate family, and ply angle increment that minimize cryotank weight while meeting structural margins. This methodology is demonstrated on a representative cylindrical cryotank model subjected to combined thermal and pressure loads, exactly matching the results of an exhaustive search for the optimum while exhibiting significant improvements in computational efficiency.

Methodology

Optimization of the cryotank design is separated into two distinct steps, run in series: (1) generating ply-level material properties and stress and strain allowables at cryogenic temperatures from the constituent (i.e., fiber and matrix) properties and (2) determining the optimal (lightest weight) ply material and stacking sequence for each region of the cryotank.

Lamina Property Determination

The first step of generating the ply-level properties and allowables utilizes the Large-scale Atomic/Molecular Massively Parallel Simulator (LAMMPS) software [7] to perform molecular dynamics (MD) simulations to obtain properties of various neat thermoplastic matrix materials at 27 °C, –183 °C, and –253 °C [8]. As described in Reference [8], these thermoplastics were modeled as purely amorphous, whereas it is well-known that polyetheretherketone (PEEK), low-melt polyaryl ether ketone (LM-PAEK), and polyetherketoneketone (PEKK) are semi-crystalline. As such, the properties of these materials should be considered estimates (likely lower bounds due to the absence of crystallinity). All potential composite laminae materials are assumed to use the AS4 carbon fiber as the reinforcement, which is treated as temperature-independent and transversely isotropic, and to have a nominal volume fraction of 0.6. The properties for the six candidate thermoplastic matrix materials and AS4 carbon fiber are shown in Table 1 and Table 2, respectively.

The NASA Multiscale Analysis Tool (NASMAT) is used to generate homogenized lamina-level properties for each of the candidate matrices at the three temperatures defined in Table 1. Each candidate lamina is assumed to have a hexagonally packed microstructure with 32 subcells in the 2-direction and 56 subcells in the 3-direction (Figure 1).

TABLE 1.—TEMPERATURE DEPENDENT CANDIDATE THERMOPLASTIC MATRIX MATERIAL PROPERTIES [8]

Material	Temperature, °C	Density, kg/m^3	E, GPa	ν	G, GPa	CTE, 10^{-6}/°C	Yield strength, MPa
PEEK	–253	1310	4.35	0.404	1.55	54.3	166
	–183	1300	3.78	0.411	1.34	55.4	133
	27	1250	2.62	0.431	0.915	67.7	81.3
Elium	–253	1240	7.32	0.324	2.76	73.9	265
	–183	1220	6.44	0.333	2.42	75.7	223
	27	1170	3.72	0.385	1.34	73.6	123
LM PAEK	–253	1300	3.47	0.391	1.25	45.1	171
	–183	1290	3.24	0.398	1.16	45.3	128
	27	1250	2.43	0.419	0.856	60.4	90.4
PEKK	–253	1300	3.29	0.341	1.23	48.1	138
	–183	1280	2.99	0.343	1.11	46.2	124
	27	1240	2.04	0.313	0.779	52.6	57.6
PEI	–253	1330	4.42	0.391	1.59	47.9	132
	–183	1310	3.68	0.409	1.31	47.3	114
	27	1270	2.48	0.413	0.876	62.8	64.6
Polyimide	–253	1320	4.80	0.375	1.75	47.1	168
	–183	1310	4.35	0.389	1.56	52.3	132
	27	1240	2.64	0.397	0.944	61.3	95.5

TABLE 2.—AS4 CARBON FIBER MATERIAL PROPERTIES

Material	E_{11}, GPa	E_{22}, GPa	ν_{12}	ν_{23}	G_{12}, GPa	CTE_{11}, 10^{-6}/°C	CTE_{22}, 10^{-6}/°C	Failure strain
AS4 carbon fiber	214.3	18.7	0.32	0.3	81.4	–0.9	7.6	0.012

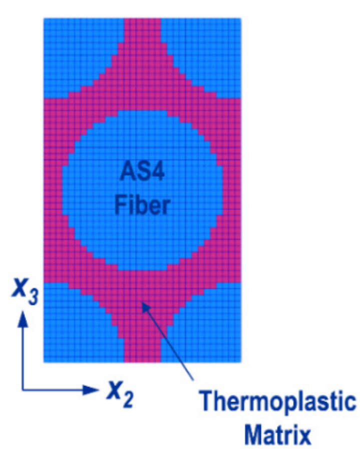

Figure 1.—Assumed microstructure for candidate laminae.

For each matrix material, at each temperature, six simulations were performed in NASMAT to determine the lamina's effective properties and allowables (uniaxial loading in the three normal and three shear directions) until failure. For fiber failure the maximum strain criterion was used, and for matrix failure the maximum stress criterion was used. The MD simulations for the matrix materials only provided a normal maximum strength (yield strength), and thus an assumed value for the shear allowable was used, calculated as

$$\sigma_{s,max} = \frac{\sigma_y}{1.65} \tag{1}$$

The factor of 1.65 was determined from measured in-house testing of PEKK, and aligns well with the von Mises criterion, which approximates normal stress as 1.732 times the shear yield stress. The lamina density was calculated using Equation (2)

$$\rho = v^f \rho^f + \left(1 - v^f\right)\rho^m \tag{2}$$

where ρ is material density, v_f is fiber volume fraction (0.6 for all laminae), and superscripts *f* and *m* are used for the fiber and matrix, respectively. Note that, although a hexagonally packed microstructure provides thermo-elastic properties that are nearly transversely isotropic, the strength predictions are generally not transversely isotropic [10]. Thus, to arrive at lamina thermo-elastic properties and strengths that were exactly transversely isotropic, the appropriate components predicted by NASMAT are averaged. As such, the effective transversely isotropic thermo-elastic properties of the lamina are calculated from the NASMAT predictions of effective properties using Equations (3) to (8)

$$E_L = E_{11} \tag{3}$$

$$E_T = \frac{1}{2}(E_{22} + E_{33}) \tag{4}$$

$$\nu_L = \frac{1}{2}(\nu_{12} + \nu_{13}) \tag{5}$$

$$G_L = \frac{1}{2}(G_{12} + G_{13}) \tag{6}$$

$$\alpha_L = \alpha_{11} \tag{7}$$

$$\alpha_T = \frac{1}{2}(\alpha_{22} + \alpha_{33}) \tag{8}$$

where E is the Young's modulus, ν is the Poisson's ratio, G is the shear modulus, α is the coefficient of thermal expansion, and subscripts L and T represent the longitudinal and transverse directions, respectively. The stress and strain allowables (σ^U and ε^U, respectively) for the lamina are calculated using Equations (9) to (12)

$$\sigma_L^U = \max(\sigma)\,|_{D=11} \tag{9}$$

$$\varepsilon_L^U = \varepsilon|_{\sigma=\sigma_L^U, D=11} \tag{10}$$

$$\sigma_T^U = \frac{1}{2}\left(\max(\sigma)\,|_{D=22} + \max(\sigma)\,|_{D=33}\right) \tag{11}$$

$$\sigma_T^U = \frac{1}{2}\left(\max(\sigma)\,|_{D=22} + \max(\sigma)\,|_{D=33}\right) \tag{12}$$

$$\tau_L^U = \frac{1}{2}\left(\max(\tau)\,|_{D=12} + \max(\tau)\,|_{D=13}\right) \tag{13}$$

$$\gamma_L^U = \frac{1}{2}\left(\varepsilon|_{\tau=\tau_L^U, D=12} + \varepsilon|_{\tau=\tau_L^U, D=13}\right) \tag{14}$$

where $D = ij$ signifies the stress-strain response from the uniaxial simulation in the ij direction.

Laminate Design Determination

For a given selected lamina, the HyperX software can be used with finite element analysis (FEA) results to down select from pre-defined candidate laminate configurations within a laminate family to rapidly determine the lowest weight laminate in each user-defined zone of the structure that meets all load case failure criteria (i.e., gives all positive margins). Laminate families are used in HyperX to ensure compatibility between adjacent laminates such that adjacent laminates are compatible for manufacturing (Figure 2).

The HyperX software offers a laminate family generator where users can specify the percentage of 0°, ± 45°, and 90° plies desired in the main stacking sequence (MSS) and the methodology of dropping plies from one candidate laminate to the next. However, for cryotank design, traditional quasi-isotropic laminates typically seen in composite structures are not ideal, due to the large mismatch in ply orientation for adjacent plies, which can promote microcracking at cryogenic temperatures. Thus, for the cryotank optimization, custom methodologies for generating laminate families were needed. Four different sets of rules for generating cryotank laminate families were created with the objective of reducing the mismatch between adjacent plies and limiting the maximum ply angle to 60°. For each ruleset, a fixed delta δ is defined as the angle increment between plies or ± ply pairs, and a total minimum number of required plies in the main stacking sequence n_{min} is set. Additionally, each ruleset contains a "thin-pack" of [± 60, 0_]$_s$ plies at the center of the laminate that is never dropped from one candidate laminate to the next. Note

Main Stacking Sequence	Zone 1	Zone 2	Zone 3
0	0		
90	90		
0	0	0	
0	0	0	0
90	90	90	90
90	90	90	90
0	0	0	0
0	0	0	
90	90		
0	0		

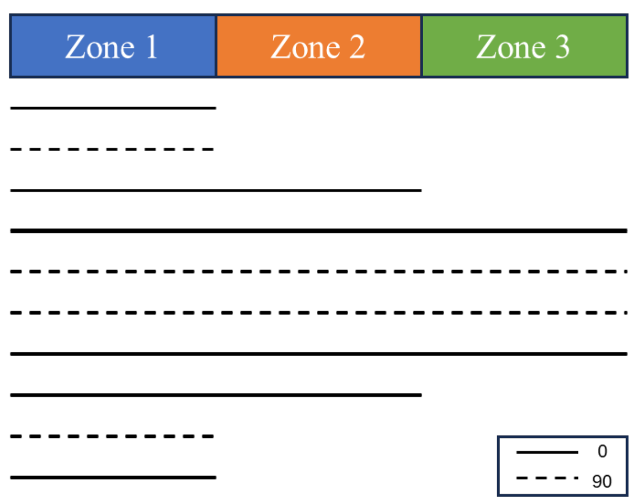

Figure 2.—Laminate families in HyperX: (a) Definition of the laminate family and (b) Schematic of zone compatibility for manufacturing.

that the underscore indicates that 0 ply is not repeated in the symmetric layup pattern. The purpose of the thin ply pack is help as a barrier against permeability by limiting the continuous through-thickness crack length compared to the standard thickness plies and increasing crack path tortuosity from thin ply to thin ply. All laminates are assumed to be symmetric, and thus are only defined up to the thin ply pack. The four rulesets are defined below:

1. Adjacent ± angle pairs, stacks of angles repeat

   In Ruleset 1, for each angle increment, δ, two plies are added to the main stacking sequence ($+\theta$ and $-\theta$), continuing every two plies until $|\theta| \geq 60°$, thus defining the stack of plies. The stack is then reversed and appended to the main stacking sequence in repetition until there are at least $n_{min}/2$ plies. The thin-ply pack is then appended to the main stacking sequence, which is then made symmetric. Figure 3(a) shows an example main stacking sequence using Ruleset 1 up to the line of symmetry. Green boxes show the forward and reversed stacks that are repeated in the main stacking sequence and the red box shows the adjacent angle pairs. For each laminate in the laminate family, ± plies are dropped from the outermost layer, resulting in a traditional triangular laminate family shape.

2. Adjacent ± angle pairs, individual angles repeat

   In Ruleset 2, the total number of ± plies for each angle from δ to θ_{max}, where θ_{max} is the maximum multiple of δ less than 60°, is calculated from n_{min}, denoted as n_{ply}. At each increment of δ, ± pairs of θ are repeated n_{ply} times, continuing until $\theta = \theta_{max}$. The thin-ply pack is then appended to the main stacking sequence, which is then made symmetric. Figure 3(b) shows an example main stacking sequence using Ruleset 2 up to the line of symmetry. Green boxes show ± pairs of each angle repeating before moving to the next increment, δ, and the red box shows the adjacent angle pairs. For each laminate in the laminate family, a ± pair from each stack is dropped, resulting in the tree-shaped laminate family.

3. Non-adjacent ± angle pairs, stacks of angles repeat

   In Ruleset 3, at each increment of δ, one angle is added to the main stacking sequence, starting from $-\theta_{max}$ to θ_{max}, defining the stack. Similar to Ruleset 1, stacks of angles are repeated until there are at least $n_{min}/2$ plies. The thin-ply pack is then appended to the main stacking sequence, which is then made symmetric. Figure 3(c) shows an example main stacking sequence using Ruleset 3 up to the line of symmetry. Green boxes show stacks of each angle repeating, and the red box shows the non-adjacent angle pairs. For each laminate in the laminate family, the outermost ply is dropped, resulting in a traditional triangular laminate family shape. Note that in this formulation, symmetry is guaranteed for each candidate laminate, but balance is not (equal number of $+\theta$ and $-\theta$ plies).

4. Non-adjacent ± angle pairs, individual angles repeat

   In Ruleset 4, the total number of ± plies for each angle from δ to θ_{max}, similar to Ruleset 2. At each increment of δ, θ is repeated n_{ply} times from $-\theta_{max}$ until θ_{max}. The thin-ply pack is then appended to the main stacking sequence, which is then made symmetric. Figure 3(d) shows an example main stacking sequence using Ruleset 4 up to the line of symmetry. Green boxes show each angle repeating before moving to the next angle increment, δ, and the red box shows the non-adjacent angle pairs. For each laminate in the laminate family, the outermost ply of each θ is dropped, resulting in the tree-shaped laminate family. Note that in this formulation, symmetry is guaranteed for each candidate laminate, but balance is not (equal number of $+\theta$ and $-\theta$ plies).

Ply	MSS	1	2	3	4	5	6	7
1	10							
2	-10							
3	20	20						
4	-20	-20						
5	30	30	30					
6	-30	-30	-30					
7	40	40	40	40				
8	-40	-40	-40	-40				
9	50	50	50	50	50			
10	-50	-50	-50	-50	-50			
11	-50	-50	-50	-50	-50	-50		
12	50	50	50	50	50	50		
13	-40	-40	-40	-40	-40	-40	-40	
14	40	40	40	40	40	40	40	
15	-30	-30	-30	-30	-30	-30	-30	-30
16	30	30	30	30	30	30	30	30
17	-20	-20	-20	-20	-20	-20	-20	-20
18	20	20	20	20	20	20	20	20
19	-10	-10	-10	-10	-10	-10	-10	-10
20	10	10	10	10	10	10	10	10
21	10	10	10	10	10	10	10	10
22	-10	-10	-10	-10	-10	-10	-10	-10
23	20	20	20	20	20	20	20	20
24	-20	-20	-20	-20	-20	-20	-20	-20
25	30	30	30	30	30	30	30	30
26	-30	-30	-30	-30	-30	-30	-30	-30
27	40	40	40	40	40	40	40	40
28	-40	-40	-40	-40	-40	-40	-40	-40
29	50	50	50	50	50	50	50	50
30	-50	-50	-50	-50	-50	-50	-50	-50
31	60	60	60	60	60	60	60	60
32	-60	-60	-60	-60	-60	-60	-60	-60
33	0	0	0	0	0	0	0	0

(a)

Ply	MSS	1	2	3	4	5	6	7
1	10							
2	-10							
3	10	10	10	10	10	10		
4	-10	-10	-10	-10	-10	-10		
5	10	10	10	10	10	10	10	10
6	-10	-10	-10	-10	-10	-10	-10	-10
7	20	20						
8	-20	-20						
9	20	20	20	20	20	20	20	
10	-20	-20	-20	-20	-20	-20	-20	
11	20	20	20	20	20	20	20	20
12	-20	-20	-20	-20	-20	-20	-20	-20
13	30	30	30					
14	-30	-30	-30					
15	30	30	30	30	30	30	30	30
16	-30	-30	-30	-30	-30	-30	-30	-30
17	30	30	30	30	30	30	30	30
18	-30	-30	-30	-30	-30	-30	-30	-30
19	40	40	40	40				
20	-40	-40	-40	-40				
21	40	40	40	40	40	40	40	40
22	-40	-40	-40	-40	-40	-40	-40	-40
23	40	40	40	40	40	40	40	40
24	-40	-40	-40	-40	-40	-40	-40	-40
25	50	50	50	50	50			
26	-50	-50	-50	-50	-50			
27	50	50	50	50	50	50	50	50
28	-50	-50	-50	-50	-50	-50	-50	-50
29	50	50	50	50	50	50	50	50
30	-50	-50	-50	-50	-50	-50	-50	-50
31	60	60	60	60	60	60	60	60
32	-60	-60	-60	-60	-60	-60	-60	-60
33	0	0	0	0	0	0	0	0

(b)

Ply	MSS	1	2	3	4	5	6	7
1	-50							
2	-40	-40						
3	-30	-30	-30					
4	-20	-20	-20	-20				
5	-10	-10	-10	-10	-10			
6	10	10	10	10	10	10		
7	20	20	20	20	20	20	20	
8	30	30	30	30	30	30	30	30
9	40	40	40	40	40	40	40	40
10	50	50	50	50	50	50	50	50
11	50	50	50	50	50	50	50	50
12	40	40	40	40	40	40	40	40
13	30	30	30	30	30	30	30	30
14	20	20	20	20	20	20	20	20
15	10	10	10	10	10	10	10	10
16	-10	-10	-10	-10	-10	-10	-10	-10
17	-20	-20	-20	-20	-20	-20	-20	-20
18	-30	-30	-30	-30	-30	-30	-30	-30
19	-40	-40	-40	-40	-40	-40	-40	-40
20	-50	-50	-50	-50	-50	-50	-50	-50
21	-50	-50	-50	-50	-50	-50	-50	-50
22	-40	-40	-40	-40	-40	-40	-40	-40
23	-30	-30	-30	-30	-30	-30	-30	-30
24	-20	-20	-20	-20	-20	-20	-20	-20
25	-10	-10	-10	-10	-10	-10	-10	-10
26	10	10	10	10	10	10	10	10
27	20	20	20	20	20	20	20	20
28	30	30	30	30	30	30	30	30
29	40	40	40	40	40	40	40	40
30	50	50	50	50	50	50	50	50
31	60	60	60	60	60	60	60	60
32	-60	-60	-60	-60	-60	-60	-60	-60
33	0	0	0	0	0	0	0	0

(c)

Ply	MSS	1	2	3	4	5	6	7
1	-50							
2	-50	-50	-50	-50	-50	-50	-50	-50
3	-50	-50	-50	-50	-50	-50	-50	-50
4	-40	-40						
5	-40	-40	-40	-40	-40	-40	-40	-40
6	-40	-40	-40	-40	-40	-40	-40	-40
7	-30	-30	-30					
8	-30	-30	-30	-30	-30	-30	-30	-30
9	-30	-30	-30	-30	-30	-30	-30	
10	-20	-20	-20	-20				
11	-20	-20	-20	-20	-20	-20	-20	-20
12	-20	-20	-20	-20	-20	-20	-20	-20
13	-10	-10	-10	-10	-10			
14	-10	-10	-10	-10	-10	-10	-10	-10
15	-10	-10	-10	-10	-10	-10	-10	-10
16	10	10	10	10	10	10		
17	10	10	10	10	10	10	10	10
18	10	10	10	10	10	10	10	10
19	20	20	20	20	20	20	20	
20	20	20	20	20	20	20	20	20
21	20	20	20	20	20	20	20	20
22	30	30	30	30	30	30	30	30
23	30	30	30	30	30	30	30	30
24	30	30	30	30	30	30	30	30
25	40	40	40	40	40	40	40	40
26	40	40	40	40	40	40	40	40
27	40	40	40	40	40	40	40	40
28	50	50	50	50	50	50	50	50
29	50	50	50	50	50	50	50	50
30	50	50	50	50	50	50	50	50
31	60	60	60	60	60	60	60	60
32	-60	-60	-60	-60	-60	-60	-60	-60
33	0	0	0	0	0	0	0	0

(d)

Figure 3.—Example cryotank laminate family definitions for $\delta = 10^\circ$ and $n_{min}/2 = 33$: (a) Ruleset 1, (b) Ruleset 2, (c) Ruleset 3, and (d) Ruleset 4. Green boxes show how angles are repeated and red boxes show angle adjacency rules.

Structural Model

To demonstrate the multiscale modeling and Bayesian optimization process within HyperX, a simple, cylindrical cryotank design (Figure 4) was considered. The cryotank has an overall length of 60 in. (1524 mm) and a height (or diameter) of 24 in. (609.6 mm). The central cylindrical section is 36 in. (914.4 mm) long, while each end has a radius of 12 in. (304.8 mm), forming the hemispherical caps or domes. This design is typical for cryogenic tanks to ensure structural integrity and pressure distribution.

The finite element model was developed in MSC/Patran and structurally analyzed using MSC/Nastran, linear solver (SOL 101). The Nastran finite element model and results (op2 file) are required inputs to HyperX. The finite element model, shown in Figure 5, consists of 20,470 nodes and 20,546 shell elements, comprised of 20,370 CQUAD4 elements and 156 CTRIA3 elements. The CTRIA3 elements, highlighted in the model, were used in regions where quad meshing was not feasible, ensuring complete surface coverage. The mesh provides adequate resolution for capturing stress/strain gradients and deformations under the applied loading. The model was constrained in all translational and rotational degrees of freedom at a single node located on the left dome, to allow the structure to deform freely under pressure and thermal loading.

All elements in the model were assigned initial composite material properties, along with appropriate material orientations following the longitudinal meridian. These initial material properties are arbitrary as they were replaced with the appropriate thermoplastic composite material properties and layup during each HyperX optimization.

A total of six combined mechanical (pressure) and thermal load cases are considered in the structural analysis, representative of realistic cryotank service conditions. In addition, the individual mechanical (three pressures) and thermal (two temperatures) load cases were evaluated for use in HyperX such that an appropriate safety factor could be employed. The 11 NASTRAN load cases are summarized in Table 3. Note that a typical liquid hydrogen tank maximum expected operating pressure (MEOP) 1035 kPa (150 psi) has been assumed.

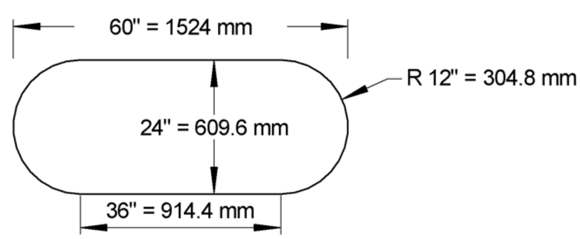

Figure 4.—Cryotank schematic.

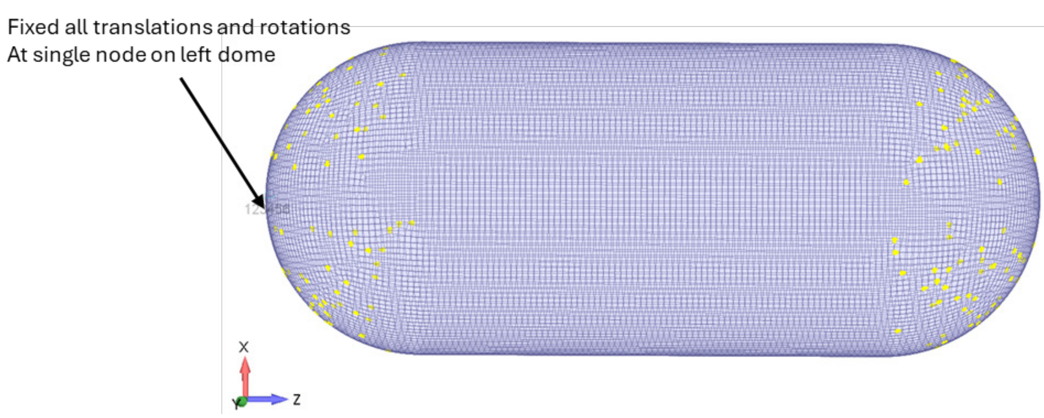

Figure 5.—Cryotank finite element model.

Static analysis of the cryotank was performed using MSC Nastran involving the 11 subcases, which combined both pressure and temperature loading conditions, shown in Table 3. As an illustration, model strain results are shown in contour plots that represent the enveloped major and minor principal strains across all load cases for a nominal quasi-isotropic IM7/8552 laminate with a thickness of 1.1176 mm. The transition zones between the cylinder and end caps show moderate strain levels while the hemispherical end caps exhibit lower strain magnitudes, as expected. The peak strain, approximately 0.01363, occurs in Load Case 2 with a combined loading of room temperature and proof pressure loading, shown in Figure 6. The minimum principal strain is –0.00752, which occurs in Load Case 5 with a combined cryo temperature and Proof pressure loading, shown in Figure 7.

TABLE 3.—CRYOTANK NASTRAN LOAD CASES

Load cases	Temperature, °C	Pressure, MPa	Temperature, °F	Pressure, psi
LC1_RT_Empty	20	0.1034	68	15
LC2_RT_Proof	20	1.448	68	210
LC3_RT_MEOP	20	1.0343	68	150
LC4_Cryo_Empty	–253	0.1034	–423.4	15
LC5_Cryo_Proof	–253	1.448	–423.4	210
LC6_Cryo_MEOP	–253	1.0343	–423.4	150
LC7_Empty_P_only	------	0.1034	--------	15
LC8_Proof_P_only	------	1.448	--------	210
LC9_MEOP_P_only	------	1.0343	--------	150
LC10_RT_T_only	20	--------	68	----
LC11_Cryo_T_only	–253	--------	–423.4	----

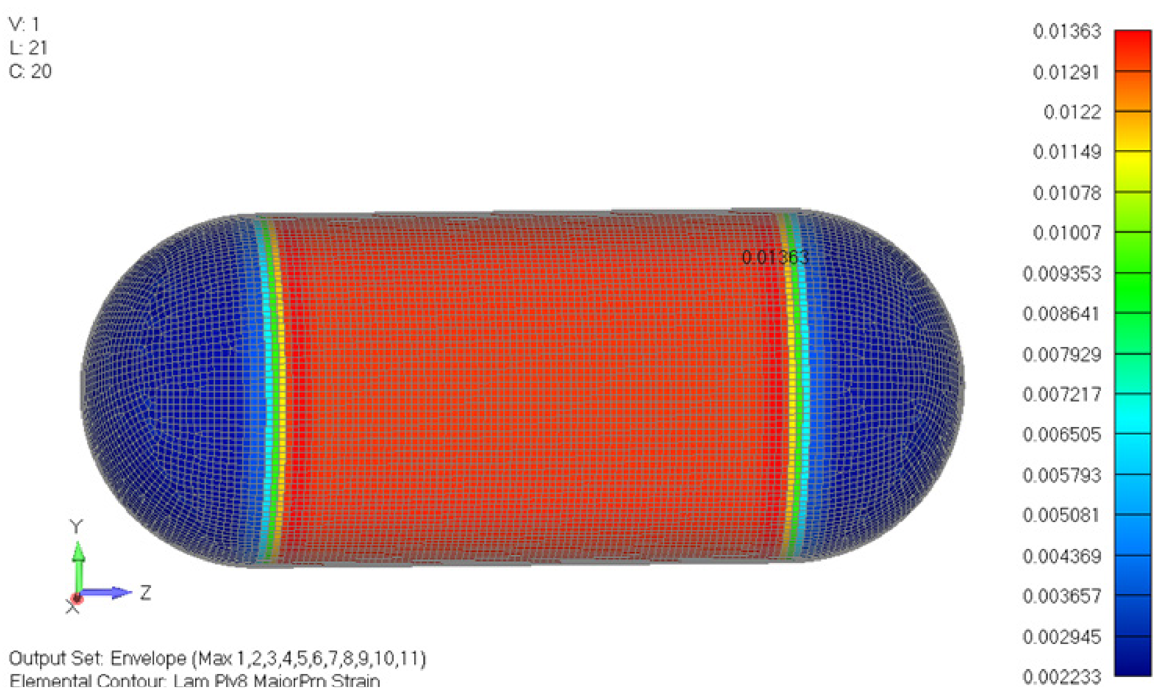

Figure 6.—Major principal strain, peak load case 2.

The NASTRAN model results are imported into the HyperX software to perform laminate optimization for the structure. The cryotank structure is separated into three zones, each of which can be assigned a unique laminate from the same laminate family for structural optimization (Figure 8). Six combined mechanical/thermal design loads, which result from combinations of load cases 7 to 11 from Table 3 are considered within HyperX, as summarized in Table 4. Note that the safety factor of 2.0 is applied only to the mechanical loading in HyperX, which is the reason for separating the thermal and mechanical load cases in the NASTRAN model.

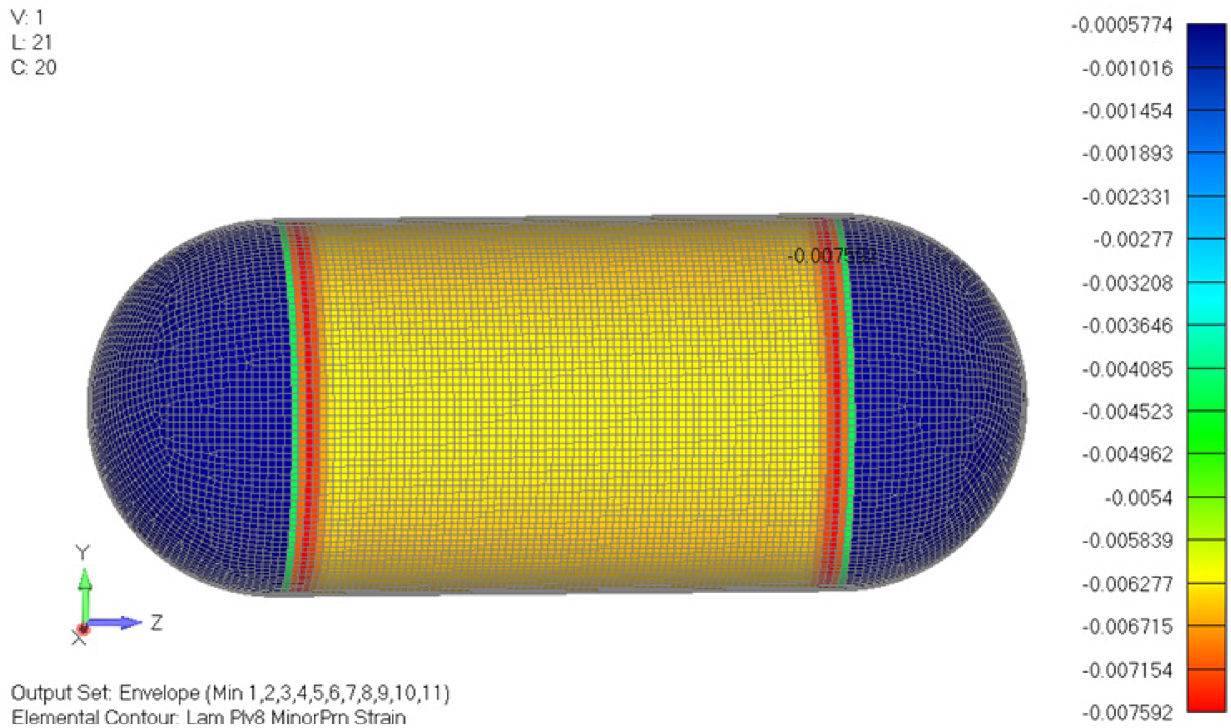

Figure 7.—Minor principal strain, peak load case 5.

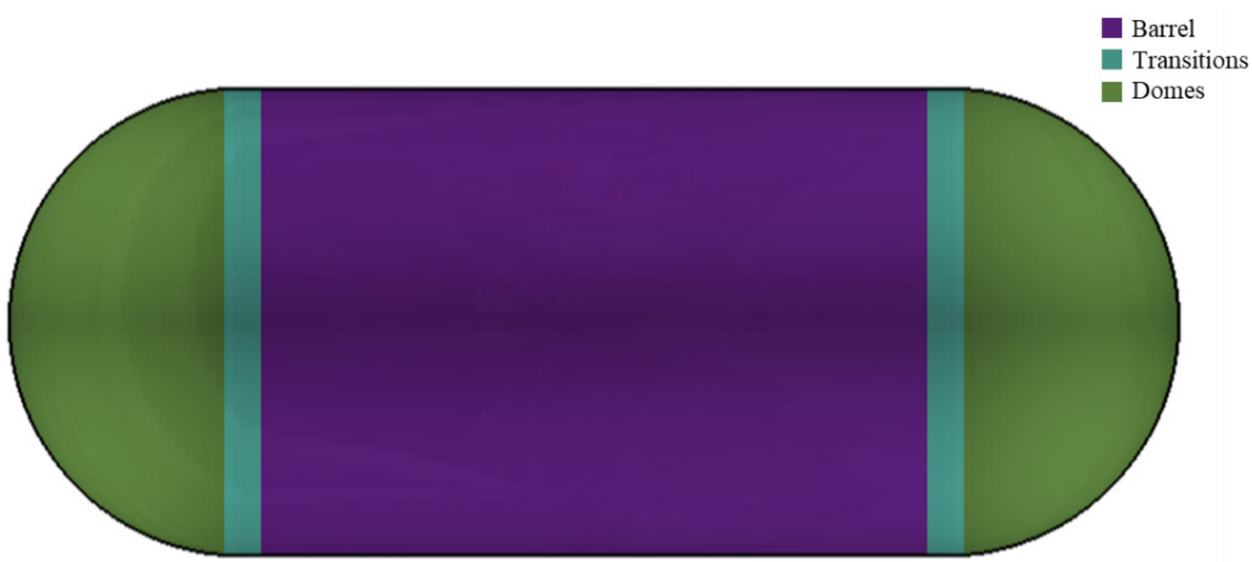

Figure 8. Cryotank zone definition in HyperX.

TABLE 4.—CRYOTANK HYPERX DESIGN LOADS
NASTRAN LOAD CASE (LC) NUMBERS REFER TO TABLE 3

Load case	Description	Temperature, °C	Safety factor
Empty RT	Combined Load: Mechanical (LC7), Thermal (LC10)	20	2
Proof RT	Combined Load: Mechanical (LC8), Thermal (LC10)	20	2
MEOP RT	Combined Load: Mechanical (LC9), Thermal (LC10)	20	2
Empty Cryo	Combined Load: Mechanical (LC7), Thermal (LC11)	–253	2
Proof Cryo	Combined Load: Mechanical (LC8), Thermal (LC11)	–253	2
MEOP Cryo	Combined Load: Mechanical (LC9), Thermal (LC11)	–253	2

Bayesian Optimization

The HyperX software is able to rapidly determine the ideal laminates in each zone of a structure, given a supplied laminate family, that minimizes the total weight of the structure. However, there is no guarantee that the user has provided HyperX with the ideal laminate family to optimize throughout the structure. Thus, if the HyperX software is combined with an advanced optimization framework for determining the best laminate family, composite structures can be rapidly optimized with regards to both material selection and laminate stacking sequence. For this work, Bayesian Optimization (BO), a sequential design strategy for optimization of complex functions, is used to determine the optimal laminate family, which is then fed to HyperX to find the optimal structural design of the cryotank. BO iteratively tries to balance exploration, or sampling the design space in areas of high uncertainty, and exploitation, or sampling in areas near the best performance of the model, to find global optima [2].

BO has five general steps to determine the optimal value of a black-box function [3]. In step 1, initial data is gathered by performing simulations or experiments that randomly sample the design space. In step 2, a surrogate model that predicts the output and uncertainty from the defined inputs is trained using the available real data (i.e., generated directly from the black-box function). For the first iteration, the initial data set is the real data. In step 3, an optimizer is employed that finds the input that maximizes the acquisition function derived from the surrogate model. In step 4, the black-box function is sampled using the optimal point found in the acquisition function, or mathematical rule that defines where to sample next, resulting in additional real data. In step 5, steps 2 to 4 are repeated with the newly added real data until a desired outcome is achieved or resources for performing simulations or experiments are exhausted.

For the cryotank design problem, the initial data set is generated by randomly selecting different combinations of laminate family rulesets, values of δ, and matrix materials. The bounds/options for each input are summarized in Table 5. The black-box function to optimize uses the laminate family ruleset and value of δ to generate the full laminate family for the candidate, and gets the temperature-dependent lamina properties associated with the selected matrix material. Both the material properties and laminate family are written to a HyperX format Excel data file, imported into the cryotank HyperX project, and applied to each zone in the structure through the HyperX Python API, which functions in the loop with the BO. The structural weight and minimum margin are also found by running the HyperX optimization in the loop via the API. The objective of the black-box function, which is to be minimized, is then calculated as

$$F = \begin{cases} W(1-M) & if\ M < 0 \\ W & if\ M \geq 0 \end{cases} \tag{15}$$

where W is the total weight of the structure and M is the minimum margin of safety. Note that in Equation (15), an additional scaling factor can be applied to the negative margin case to increase or decrease the penalty for negative margin simulations. Increasing the scaling factor, thus heavily punishing negative margins, will push the optimization away from the zero margin case, which will be close to the minimum weight solution. In this work, the scaling factor was not studied because the HyperX software automatically returns the lowest weight solution with all positive margins, and the supplied main stacking sequence for each generated laminate family always returned positive margins. The negative margin function would only be used if all provided laminates in the laminate family resulted in a negative margin. All provided rulesets to the BO algorithm gave initial main stacking sequences well above the required number of plies to ensure no negative margins would be returned from the HyperX result.

The Bayesian Back End (BayBE) framework [4] was used to perform the structural optimization in Python. Each of the input parameters in Table 5 was treated as a categorical parameter, with each option represented as a string of an integer value using one-hot encoding, such that only discrete values were allowed without interpretation between elements of each list. Single-objective optimization was selected to minimize a numerical target, and the expected improvement acquisition function was used. A hybrid recommender for exploration (sampling where predicted uncertainty is high) and exploitation (sampling where predicted value is optimal) was created by using the two phase meta-recommender and the Naïve Hybrid space recommender built into BayBE, which decides how the surrogate and acquisition function values are used to recommend the next batch of data points to evaluate using the black box function. For both the initial data set and each iteration of BO, the batch size (i.e., number of data points to evaluate using the physics-based workflow, recommended by the BO algorithm) was set to 10. The maximum number of iterations was set to 50 to ensure that an optimal value was achieved.

Results and Discussion

Using the BayBE framework, the optimal material and stacking sequence for the cryotank structure was found in seven iterations of the BO algorithm (Figure 9). In the figure, the red line represents the minimum weight found across all previous iterations (global minimum), while the blue line represents the minimum weight at the current configuration, demonstrating the explorative nature of the hybrid recommender. The true minimum was determined by conducting an exhaustive search of the full-factorial

TABLE 5.—CRYOTANK OPTIMIZATION INPUT PARAMETERS

Input	Type	Options
Laminate Family Rule Set	Categorical	1 – Ruleset 1 2 – Ruleset 2 3 – Ruleset 3 4 – Ruleset 4
$\boldsymbol{\delta}$	Categorical	Integer between 3 and 15
Matrix	Categorical	0 – PEEK 1 – Elium 2 – LM PAEK 3 – PEKK 4 – PEI 5 – Polyimide

312 combinations of matrix material, δ, and laminate family ruleset. This true minimum matched the weight and configuration found using the BO algorithm after 7 iterations, summarized in Table 6. Note that in Table 6, the safety factor for each load case is built into the design load definition in HyperX. Thus, a structure that perfectly meets the specified safety factor would have a margin of 0.

The resultant selected laminates from the ideal laminate family are shown in Figure 10. From the figure, it can be observed that the ply thickness in the barrel (41 plies, including 5 thin plies) is ~3.6 times larger than that of the transitions and domes (13 plies, including 5 thin plies). Additionally, HyperX selected the same laminate for both the transition and dome regions. Both observations are expected, since the barrel is expected to carry the largest portion of the pressure loads and the load variation between the transition and domes is relatively small compared to the barrel.

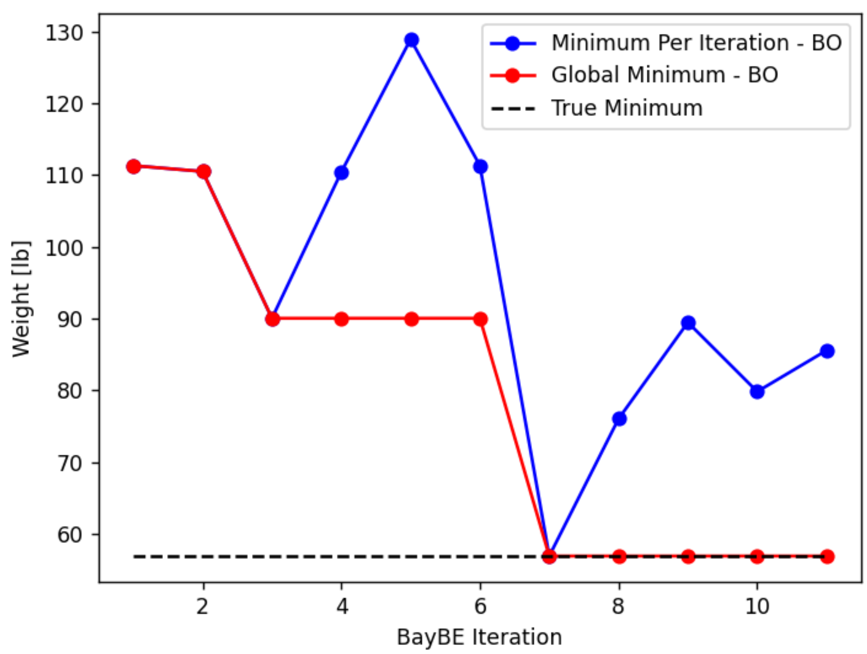

Figure 9.—Cryotank Bayesian Optimization performance. Only the first 11 iterations are shown since optimal value was reached and no further model improvement is possible.

TABLE 6.—OPTIMAL STRUCTURAL DESIGN OF THE CRYOTANK

Parameter	Result
Matrix material	Elium
δ	14°
Laminate family ruleset	Ruleset 1
Weight, lb	59.96
Minimum margin	0.0585

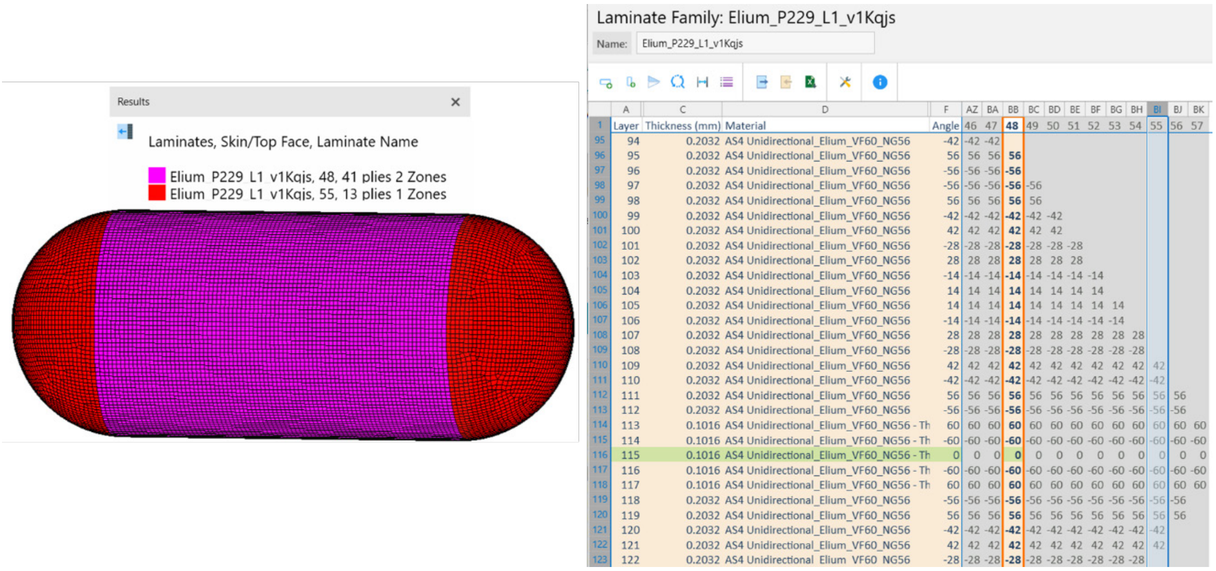

	A	C	D	F	AZ	BA	BB	BC	BD	BE	BF	BG	BH	BI	BJ	BK
1	Layer	Thickness (mm)	Material	Angle	46	47	48	49	50	51	52	53	54	55	56	57
95	94	0.2032	AS4 Unidirectional_Elium_VF60_NG56	-42	-42	-42										
96	95	0.2032	AS4 Unidirectional_Elium_VF60_NG56	56	56	56	56									
97	96	0.2032	AS4 Unidirectional_Elium_VF60_NG56	-56	-56	-56	-56									
98	97	0.2032	AS4 Unidirectional_Elium_VF60_NG56	-56	-56	-56	-56	-56								
99	98	0.2032	AS4 Unidirectional_Elium_VF60_NG56	56	56	56	56	56								
100	99	0.2032	AS4 Unidirectional_Elium_VF60_NG56	-42	-42	-42	-42	-42	-42							
101	100	0.2032	AS4 Unidirectional_Elium_VF60_NG56	42	42	42	42	42	42							
102	101	0.2032	AS4 Unidirectional_Elium_VF60_NG56	-28	-28	-28	-28	-28	-28	-28						
103	102	0.2032	AS4 Unidirectional_Elium_VF60_NG56	28	28	28	28	28	28	28						
104	103	0.2032	AS4 Unidirectional_Elium_VF60_NG56	-14	-14	-14	-14	-14	-14	-14	-14					
105	104	0.2032	AS4 Unidirectional_Elium_VF60_NG56	14	14	14	14	14	14	14	14					
106	105	0.2032	AS4 Unidirectional_Elium_VF60_NG56	14	14	14	14	14	14	14	14	14				
107	106	0.2032	AS4 Unidirectional_Elium_VF60_NG56	-14	-14	-14	-14	-14	-14	-14	-14	-14				
108	107	0.2032	AS4 Unidirectional_Elium_VF60_NG56	28	28	28	28	28	28	28	28	28	28			
109	108	0.2032	AS4 Unidirectional_Elium_VF60_NG56	-28	-28	-28	-28	-28	-28	-28	-28	-28	-28			
110	109	0.2032	AS4 Unidirectional_Elium_VF60_NG56	42	42	42	42	42	42	42	42	42	42	42		
111	110	0.2032	AS4 Unidirectional_Elium_VF60_NG56	-42	-42	-42	-42	-42	-42	-42	-42	-42	-42	-42		
112	111	0.2032	AS4 Unidirectional_Elium_VF60_NG56	56	56	56	56	56	56	56	56	56	56	56	56	
113	112	0.2032	AS4 Unidirectional_Elium_VF60_NG56	-56	-56	-56	-56	-56	-56	-56	-56	-56	-56	-56	-56	
114	113	0.1016	AS4 Unidirectional_Elium_VF60_NG56 - Th	60	60	60	60	60	60	60	60	60	60	60	60	60
115	114	0.1016	AS4 Unidirectional_Elium_VF60_NG56 - Th	-60	-60	-60	-60	-60	-60	-60	-60	-60	-60	-60	-60	-60
116	115	0.1016	AS4 Unidirectional_Elium_VF60_NG56 - Th	0	0	0	0	0	0	0	0	0	0	0	0	0
117	116	0.1016	AS4 Unidirectional_Elium_VF60_NG56 - Th	-60	-60	-60	-60	-60	-60	-60	-60	-60	-60	-60	-60	-60
118	117	0.1016	AS4 Unidirectional_Elium_VF60_NG56 - Th	60	60	60	60	60	60	60	60	60	60	60	60	60
119	118	0.2032	AS4 Unidirectional_Elium_VF60_NG56	-56	-56	-56	-56	-56	-56	-56	-56	-56	-56	-56	-56	
120	119	0.2032	AS4 Unidirectional_Elium_VF60_NG56	56	56	56	56	56	56	56	56	56	56	56	56	
121	120	0.2032	AS4 Unidirectional_Elium_VF60_NG56	-42	-42	-42	-42	-42	-42	-42	-42	-42	-42	-42		
122	121	0.2032	AS4 Unidirectional_Elium_VF60_NG56	42	42	42	42	42	42	42	42	42	42	42		
123	122	0.2032	AS4 Unidirectional Elium VF60 NG56	-28	-28	-28	-28	-28	-28	-28	-28	-28	-28			

Figure 10.—Optimal Laminates in Each Zone of the Cryotank

Overall, the employed methodology for selecting the optimal material, laminate family, and individual laminates significantly outperformed the exhaustive search in time taken do reach the optimal solution (~1 hr for BO vs. ~4 hr for exhaustive search). Although the HyperX optimization is fast in each case, on the order of seconds to minutes, each iteration for both methods require generating the laminate family and writing and importing an Excel file into HyperX with the materials and full laminate family definition. Both methods could see increased performance by importing multiple materials and laminate families at once in a single file. It should also be noted that the chosen design space for the optimization problem was relatively small; given the defined rulesets, range of δ, and available materials, only 312 unique laminate families (~6500 laminate candidates for each of the three zones) were made available to the BO process. The design space could be increased substantially by:

1. Treating δ as a continuous variable
2. Adding more laminate family rulesets
3. Adding more matrix materials to the constituent database
4. Adding more fiber materials to the constituent database, or
5. Considering different microstructures (volume fraction and packing)

Option 1 would significantly expand the design space by changing the BO input type to numerical from categorical for δ, but would likely result in much longer solution times without any gain structural performance/weight, since it is highly unlikely any actual structure will contain non-integer ply angles. Option 2 is the least expensive method of expanding the design space, and it could potentially have a significant impact on the final design. Additional candidate laminate families could be variations of the existing rules, such as using non-constant steps between angles or considering various methods for dropping plies from one laminate to another, or they could be created using generative optimization algorithms. In addition, new or different classes of laminate families, that are not based on angle steps, could be considered (e.g., quad or Double-Double laminates [11]). Options 3 and 4 are both feasible for expanding the design space, but are more expensive than option 2. For matrix materials, running the MD simulations to predict the temperature-dependent properties takes approximately 2 days of computational time per material. Because the carbon fiber materials are typically not temperature-dependent, the computational cost for adding additional materials to the database is low, but does rely on data availability (both mechanical properties and failure allowables). Option 5 is inexpensive in terms of computational time, but the microstructure is often a result of the manufacturing process rather than an input design variable.

Conclusions

This study demonstrated an integrated methodology for the design and optimization of thermoplastic composite cryotanks under cryogenic operating conditions. By coupling molecular dynamics simulations with micromechanics modeling in NASMAT, temperature-dependent lamina properties were obtained from constituent material data, enabling accurate prediction of ply-level response. These properties were incorporated into laminate family definitions within HyperX, allowing efficient structural optimization across cryotank zones. Bayesian optimization was then used to intelligently sample the design space, rapidly converging to an optimal configuration that matched the global minimum obtained by exhaustive search while requiring only a fraction of the computational effort.

The optimized cryotank design selected Elium as the matrix material, a 14° ply angle increment, and laminate family Ruleset 1, resulting in a 59.96 lb structure with positive margins under all combined cryogenic load cases. The efficiency gains of BO, achieving convergence in ~1 hr compared to ~8 hr for exhaustive search, illustrate the promise of this approach for accelerating composite structural design. Importantly, the methodology is extensible: expanding the design space to include additional laminate rules, alternative matrix and fiber materials, or different microstructures could yield further improvements in structural performance.

Overall, the framework presented here provides a pathway for systematic and computationally efficient design of cryogenic composite tanks. By integrating molecular-scale property prediction, multiscale homogenization, structural optimization, and Bayesian search strategies, this approach offers both accuracy and scalability for aerospace composite applications. Future work should extend the design space, validate optimized laminates experimentally under cryogenic loading, and explore automated coupling of generative laminate design with Bayesian optimization to further accelerate discovery of high-performance cryotank configurations.

References

[1] M. Saha and R. Sullivan, “A review on gas permeability of polymer matrix composites for cryogenic applications,” *Composites Part B: Engineering,* vol. 271, no. 111699, 2024.

[2] B. Shahriari, K. Swersky, Z. Wang, R. P. Adams and N. de Freitas, “Taking the Human Out of the Loop: A Review of Bayesian Optimization,” *Proceedings of the IEEE,* vol. 104, no. 1, pp. 148-175, 2016.

[3] J. Stuckner, P. Toma, J. Goodin, B. Hearley and S. Xie, “Benchmarking Bayesian Optimization Frameworks and Acquisition Strategies for Materials Discovery and Autonomous Laboratories,” *submitted for publication.*

[4] M. Fitzner et al., “BayBE: a Bayesian Back End for experimental planning in the low-to-no-data regime,” *Digit. Discov.,* 2025.

[5] Collier Aerospace, “HyperX,” [Online]. Available: https://collieraerospace.com/.

[6] E. J. Pineda, B. A. Bednarcyk, T. M. Ricks, S. M. Arnold and G. Henson, "Efficient multi-scale recursive micromechanics of composites for engineering applications," *Internaitonal Journal for Multiscale Computational Engineering,* vol. 19, no. 4, 2021.

[7] Sandia National Laboratories, "LAMMPS Molecular Dynamics Simulator," [Online]. Available: https://www.lammps.org.

[8] S. S. Baman, S. Patil, K. Kashmari, B. Jansen, J. Hinkley, J. H. Kang and G. M. Odegard, "Investigation of material properties of thermoplastic polymer materials at cryogenic temperatures using molecular dynamics," *NASA/TM in press.*

[9] National Aeronautics and Space Administration, "NASA Multiscale Analysis Tool (NASMAT) version 4.0," [Online]. Available: http://software.nasa.gov/software/LEW-20650-1.

[10] J. Aboudi, S. Arnold and B. Bednaryck, Practical Micromechnaics of Composite Materials, Oxford, UK: Elsevier, 2021.

[11] S. Tsai, "Double-Double A New Perspective on the Manufacture and Design of Composite," *Composites Design Group, Dept. Aeronatics & Astronautics, Standford University, Stanford, CA, 2022.*